Bioelectrochemistry 139 (2021) 107740

Contents lists available at ScienceDirect

Bioelectrochemistry

journal homepage: www.elsevier.com/locate/bioelechem

Bio-nanocomposite based highly sensitive and label-free electrochemical immunosensor for endometriosis diagnostics application

Thangapandi Kalyani [a], Arumugam Sangili [a,b], Amalesh Nanda [a], Sengodu Prakash [c], Ajeet Kaushik [d,*], Saikat Kumar Jana [a,*]

[a] Department of Biotechnology, National Institute of Technology, Papum Pare 791112, Arunchal Pradesh, India
[b] Department of Chemical Engineering and Biotechnology, National Taipei University of Technology, Taipei 10608, Taiwan
[c] Department of Chemistry, Alagappa University, Karaikudi 630003, Tamilnadu, India
[d] NanoBioTech Laboratory, Department of Natural Sciences, Division of Sciences, Art, & Mathematics, Florida Polytechnic University, Lakeland FL-33805, USA

ARTICLE INFO

Article history:
Received 17 August 2020
Received in revised form 30 December 2020
Accepted 5 January 2021
Available online 11 January 2021

Keywords:
Bio-nanocomposite
Nano-sensors
Immune-sensing
Electrochemical biosensor
Endometriosis
CA19-9 biomarker
Diagnostics composite

ABSTRACT

In this research, for the first time, a bio-nanocomposites based highly sensitive and label-free electrochemical immunosensor is reported with the aim of endometriosis diagnostics application. Multiwalled carbon nanotube and magnetite nanoparticle (MWCNT-Fe_3O_4) was dispersed in chitosan (CS) to fabricate a bio-nanocomposite to immobilize very monoclonal specific antibody (via cross-linking using glutaraldehyde) for selective electrochemical immuno-sensing of carbohydrate antigen 19–9 (CA19-9), a potential biomarker for endometriosis diagnostics. Well-characterized Anti-Abs_{CA19-9}/CS-MWCNT-Fe_3O_4 immune-electrode fabricated on glassy carbon electrode (GCE) successfully detect CA 19–9 and exhibited a high sensitivity as (2.55 μA pg^{-1} cm^{-1}), a detection limit of 0.163 pg mL^{-1}, detection range from 1.0 pg mL^{-1} to 100 ng mL^{-1}. Our fabricated electrochemical Abs_{CA19-9}/CS-MWCNT-Fe_3O_4 immunosensor performed CA19-9 sensing in physiological range and at a very level which suggest it application for early-stage diagnostics, diseases monitoring, and optimization of therapy. To claim the clinical application, our sensor was tested using real samples and sensing performance was validated using enzyme-linked immune-sorbent assay (ELISA). The results of the studies projected Abs_{CA19-9}/CS-MWCNT-Fe_3O_4 electrochemical CA19-9 immunosensor as a potential and affordable alternate of conventional techniques like ELISA. We believe that our fabricated sensor can be the plane of a disease's management program due to affordable, rapid, label-free, and sensitive detection of a targeted biomarker.

1. Introduction

Endometriosis is one of the major frequent gynecological diseases which affects around 150 million women annually. As a consequence, this disease is more prominent during their reproductive age wherein endometrial tissue growing outside the uterus where non/semi-invasive based diagnosis is challenging for endometriosis [1]. Moreover, most of the endometriosis is diagnosed at an advanced stage, resulting in a high possibility of infertility and increase the rate of endometrial cancer. Generally, the Cancer Antigen 125 (CA125) assay is mostly used for endometriosis patients that commonly have an abnormally elevated level of CA125 antigen in serum (>35U mL^{-1}) due to progression of the disease [2]. However, CA125 is not a suitable biomarker for endometriosis due to the lack of sensitivity and specificity. On the other hand, CA19-9 was also emerged as a potential endometriotic biomarker due to higher sensitivity and specificity [3–5]. Thus, CA19-9 has undergone little investigation for biosensor design in the domain of endometriosis; hence it can stand to be an eminent biomarker for endometriosis diagnosis. Nowadays, technology is necessary to develop platforms for highly sensitive and direct measurement of protein levels in the clinical sample using non/semi- invasive manner [6]. Several diagnostic techniques are available for the preparation of immunosensor such an ELISA [7,8], fluorescence [9], piezoelectric [10–12], surface plasmon resonance [13,14], and electrochemical techniques [15,16]. Electrochemical immunosensors have newly emerged and gained more attention due to their advantages such as high sensitivity, miniaturization, low-cost,

* Corresponding authors.
E-mail addresses: akaushik@floridapoly.edu (A. Kaushik), saikatmicro4@gmail.com (S. Kumar Jana).

https://doi.org/10.1016/j.bioelechem.2021.107740
1567-5394/

convenience and high compatibility than other techniques [15,17,18]. An antibody is commonly used as a capture factor in immunosensor for the detection of antigen. So, proper immobilization of antibodies on the surface of the transducer is most significant. This necessity is mostly satisfied by controlling the molecular construction of micro/nanostructured composite [6]. Recently, multiwalled carbon nanotube (MWCNT) and chitosan (CS) composites have been given more attention in biosensor applications because of their synergic effects such as high chemical stability and excellent mechanical strength, along with high cohesive property between antibodies and the target analyt [19–22]. Moreover, CS is a natural, linear polysaccharide polymer; it has been shown to interact with MWCNTs to form stable dispersions, but it has shown the poor electroactive property [23–25]. Magnetite (Fe_3O_4) materials are widely used in analytical chemistry due to their attractive chemical and physical properties [26–30]. Also, it has super-paramagnetic property, biocompatibility, good electrocatalytic activity, and low toxicity and used as an attention-grabbing material for the immobilization of biomolecules [19,20,31,32]. The significant property of Fe_3O_4 is their facility to give a good microenvironment for biomolecules such as proteins to exchange electrons directly with an electrode [1], accordingly improving the sensitivity of electrochemical biosensors. Intrinsic enzyme mimetic activity of Fe_3O_4 like to that natural peroxidase, and acted as natural peroxidase to oxidize organic substrates has been proved and developed H_2O_2 and glucose biosensor by colorimetric method [33,34]. The CS capping MWCNT-Fe_3O_4 composite on the modified GC electrode enhances the stability of the electrode surface and effective immobilization of the antibody. Therefore, earlier some research efforts were made on CS-MWCNT-Fe_3O_4 bio-nanocomposite applied to different types of sensing application [35–39]. They are simple processes, high sensitivity, and short detection time, even though these sensors have problems with low conductivity of the sensing materials and uneven dispersion of composite in the solvent. To improve the conductivity as well as dispersion ability, a little amount of PDDA solution in composites is blended. Moreover, after extensive literature review, it was found that there is no research article published on detecting of CA19-9 in endometriosis using an electrochemical biosensor. This motivates to establishment biosensor for the detection of CA19-9 in endometriosis using a CS-MWCNT-Fe_3O_4 based electrochemical sensor.

In this manuscript, for the first time, a label-free electrochemical immunosensor for CA 19–9 detection is developed with an effective and efficient endometriosis diagnostics application. A film of bio-nanocomposite of CS-MWCNT-Fe_3O_4/GC nanocomposite was fabricated onto glassy carbon (GCE) to immobilize monoclonal CA19-9 antibody for the selective capturing of CA19-9 antigen selectively and at a very low level. Such fabricated CS-MWCNT-Fe_3O_4/GC platform provides a microenvironment desired by antibody to get immobilize via binding between CS and Fc region using glutaraldehyde as a cross-linker. Besides, CS supportive antibody immobilization, Fe_3O_4 provide stability to chitosan and MWCNT enhances charge transport between electrolyte-immunocomplex to bio-nanocomposite to the working electrode during immunosensing. This electrochemical immunosensor exhibited variation in magnitude to electrical signal on adding CA-19–9 antigen, recorded using a square wave voltammetry (SWV) technique in the presence of redox marker $[Fe(CN)_6]^{3-/4-}$ solution. The remarkable sensing outcomes of this sensor mainly high sensitivity and low limit of detection compared are better than other reported sensors (Table 1). To claim the clinical application, herein reported electrochemical CA-19–9 immunosensor was tested in real serum samples and sensing outcomes were validated using ELISA techniques. Such calibrated and validated CA19-9 immunosensor has the potential to promote for clinical application to achieve, affordable endometriosis diagnostics.

2. Experimental section

2.1. Materials

Multi-walled carbon nanotube (MWCNT, ≥96%), chitosan (CS, ≥75%), poly-diallyl dimethylammoniumchloride (PDDA, 20 wt%. in water), ferric chloride ($FeCl_3{\cdot}H_2O$, ≥97%), sodium acetate trihydrate (NaAc, ≥99%), cetyltrimethylammonium bromide (CTAB), ethylene glycol (EG,≥99.8%), disodium hydrogen phosphate (Na_2HPO_4, ≥99%) potassium chloride (KCl, ≥99%), glutaraldehyde (Glu, 50 wt% in water), and sodium dihydrogen phosphate (NaH_2PO_4, ≥99%) were purchased from Sigma Aldrich, India. Bovine serum albumin (BSA), monoclonal anti-CA19-9 antibody (Abs_{CA19-9} or Ab,sc-517448), cancer antigen (CA125), human recombinant carbohydrate antigen 19–9 (CA 19–9, MBS2011087), carcinoembryonic antigen (CEA), and alpha-fetoprotein (AFP) were bought from MyBio Source. All solutions were prepared using Millipore water (Millipore Sigma STMSV00US) or according to the instruction manual given by the respective company. Antigen and antibody noted as Ag and Ab, respectively.

XRD studies were performed, which analyzed the crystalline structure by PANalytical X'Pert PRO diffractometer using Cu Kα (λ = 1.5417 Å) radiation in the 2θ range from 10 to 80°. Again, the morphology was determined by transmission electron microscopy (TEM; JEOL JEM-2100F) and operated at an acceleration voltage of 200 kV. The chemical surface characterization of the composite was examined by FT-IR spectrometer (CH 1000C, FT/IR-6600), and the frequency range from 4000 to 400 cm^{-1}. The spectra were obtained at room temperature with the KBr pellet. Sonication was done by the ultrasonic cleaner (Aczel). The electrochemical analysis was performed on Bio-Logic Science Instrument (France) with a conventional three-electrode system containing glassy carbon electrode (GCE) as a working electrode, Ag/AgCl in 0.1 M KCl as a reference electrode, and platinum (Pt) wire as a counter electrode. The glassy carbon electrode was electrochemically characterized by CV, EIS, and SWV. The CV (scan rate 0.02 Vs^{-1}) and SWV [pulses height (25 mV), pulses width (50 ms), and step height (10 mV)] measurements were carried out a potential between –0.1 and 0.8 V in 5 mM $[Fe(CN)_6]^{3-/4-}$/0.1 M KCl solution with 0.05 M PBS electrolyte.

2.2. Preparation of CS functionalized MWCNT incorporation of Fe_3O_4 bio-nanocomposite

First, Fe_3O_4 NPs were synthesized using a solvothermal reaction [40]. Then, 1.5 g of $FeCl_3{\cdot}6H_2O$, 1.0 g of CTAB, and 2.0 g of sodium acetate were added into 40 mL EG, and the mixture was stirred for 30 min at ambient temperature to make a homogenous solution. It was shifted to a 50 mL Teflon-lined stainless-steel for 12 h at 180 °C. The black precipitate was obtained, separated, and washed five times with water and ethanol by using an external magnet. 25 mg of MWCNT was dispersed with 10 mL water using ultrasonication. 100 mg of Fe_3O_4 NPs was added into the MWCNT dispersed solution under stirring for 20 min and chitosan solution (200 mg chitosan dissolved in 20 mL of 0.2% acetic acid) was mixed dropwise. The mixture was stirred for 2 h at room temperature and the composite was centrifuged and washed three times with distilled water. The products were dried at 50 °C by vacuum oven. Furthermore, 1 mg of CS-MWCNT-Fe_3O_4/GC composite and 10 μL of PDDA solution (20 wt% PDDA in water) were dispersed in 1 mL of water for the subsequent use of electrochemical sensor.

Table 1
Comparison of different analytical methods for the detection of CA 19–9.

Electrode	Method	Linear range (U mL^{-1})	LOD (U mL^{-1})	Refs.
AuPtNCs[a]	DPV[i]	0.05–50	0.03	[48]
Antibody-AuNp-G-quadruplex/he[b]	CLIA[j]	0.025–1.00	0.16	[49]
Au@Pd-Gra/Thi-Ab2/HRP[d]	DPV	0.015–150	0.006	[50]
nanoFe_3O_4@GO[e]	ECL[k]	0.001–5	0.0005	[51]
TiO_2NWs/Au/CdSe@ZnS[f]	PEC[l]	0.01–200	0.0039	[52]
Ag@BSA[g]	ECL	0.0005–150	0.0002	[53]
CeO_2/FeOx@mC500[h]	EIS[m]	0.0001–10	0.00001	[54]
MWCNT-Pt-luminol	ECL	0.0001–10	0.000046	[55]
Anti-CA19-9_2/Envision/Au*	SV[n]	0.005–100	0.0003	[56]
CS-MWCNT-Fe_3O_4*	**SWV**	**0.001–100**	**0.000163**	**Present work**

[a]gold-platinum nanocalliandras, [b]anitibody-AuNp-G-quadruplex/hemin, [c]carbon quantum dots/gold nanocomposite, [d]gold @ palladium-graphene thionine secondary antibody/horseradish, [e]magnetic graphene oxide,[f]TiO_2Nano wires/Au/CdSe@ZnS,[g]Bovine serum albumin, [h]cerium-ferric oxides nanoparticles embedded within mesoporous carbon matrix, [i]differential pulse voltammetry, [j]chemiluminescent immunoassays, [j]fluorescence immunoassay, [k]electrochemiluminescence, [l]photoelectrochemical immunoassay, [m]electrochemical impedance spectroscopy, [n]stripping voltammetry, * The linear range and LOD both are ng mL^{-1}

PDDA is repeating units bear an electrolyte group, which dissociated in water and resulted as charged, and their properties are similar to electrolytes and polymers. The PDDA solutions are also electrically conductive [41]. Prakash et al. developed the uric acid sensor based on the PDDA electrolytes because of its electroconductive nature and electrostatic interaction with charged molecules [42,43]. Therefore, PDDA is used to our electrochemical biosensor analysis for improving the ionic and electronic conductivity of sensor materials.

2.3. Fabrication process of CS-MWCNT-Fe_3O_4 based immune-electrode

In the first step, the GCE was polished with 0.3 μm alumina powder, cleaned thoroughly with ethanol and Millipore water. 8.0 μL of CS-MWCNT-Fe_3O_4 composite solution (1.0 mg of the CS-MWCNT-Fe_3O_4 dispersed in 1 mL DI water) was dropped on the GCE surface and then dried at 50 °C. In the second step, the fabrication step of the immunosensor is presented in Scheme 1. Initially, the composite modified electrodes were dipped into 2% of Glu aqueous solution for 2 h to activate amino groups on the chitosan composite (CS-MWCNT-Fe_3O_4). CA19-9 antibody (15 μg of CA19-9 antibody in 1 mL of 5 mM PBS solution, pH 7.4) was dipped onto activated chitosan composite via Glu cross-linking. The two functional –CHO groups of glutaraldehyde react with $–NH_2$ sites on the chitosan to aid bonding of the antibody to chitosan. Next, the electrodes were washed with water to remove the excess Glu molecule.

Then, the modified electrode was incubated with CA19-9 antibody solution for 45 min and subsequently washed with 5 mM PBS (pH 7.4) to remove the excess of CA19-9. Afterward, the modified electrode was dipped with 1% BSA for 30 min to prevent any possible remaining active spots against non-specific interaction. Finally, the fabricated immunosensor was assigned to detect CA19-9 antigen and this experiment was carried out at 35 °C for 30 min. Scheme 1 has representation of a label-free electrochemical immunosensor fabrication for the detection of CA 19–9 biomarker.

2.4. Blood sample collection and processing to detect CA19-9 using immunosensor

This women's health-related research project was conducted at the National Institute of Technology, Arunachal Pradesh, India, which was approved by the Department of Science & Technology (DST), Science and Engineering Research Board (SERB) team. The institutional scientific ethical committee was approved [Proposal Number: NIT (A.P)/R&D/Project/11–12/1/Vol.2/IEC-02, Approval date 27/09/2016] for this study, and the sample was collected from Pratiksha Hospital, Guwahati, Assam, India. Written consent was obtained at the time of blood sample collection from the patients who were selected for the study. Women included in the study did not receive any medical or hormonal treatment during the last three months. Moreover, women with a prior history of any gynecological surgery including chocolate cyst, lower pelvic, and abdominal surgery with other possible causes of pain or pelvic pathology including pelvic tuberculosis were excluded from the study. Venous blood samples collation, process, and storage procedures were described previously [44,45].

3. Result and discussion

3.1. Evaluation of CS-MWCNT-Fe_3O_4 bio-nanocomposites structure

The phase purity and crystalline structure of the Fe_3O_4 NPs and CS-MWCNT-Fe_3O_4 were confirmed by XRD analysis as exposed in Fig. 1A. The XRD diffraction peaks at 2θ = 30.18, 35.67, 43.38, 57.01, and 62.72° may be attributed to the (220), (311), (400), (511) and (440) crystal planes, which are consistent with magnetite Fe_3O_4 cubic inverse spinel (JCPDS No. 86–1335). This result indicates the successful formation of Fe_3O_4 NPs. The XRD analysis of CS-MWCNT-Fe_3O_4, shows all characteristic peaks of Fe_3O_4 have appeared and the intensity of diffraction peak was slightly decreased our prepared composite. The results demonstrated that the Fe_3O_4 was successfully anchored on the outside of MWCNT-CS [45].

$$D = \frac{0.89\lambda_{K\alpha}}{\beta_{2\theta} Cos\theta_{max}} \quad (1)$$

where D is denoted as the particle size of theFe_3O_4 NPs, θ_{max} is denoted as diffraction angle, $\lambda_{K\alpha}$ is denoted as wavelength (Cu K$\alpha\lambda_{K\alpha}$ = 1.54 Å), and $\beta_{2\theta}$ is denoted as the full width at half maximum. The mean particle size of Fe_3O_4 NPs is 26.9 nm which is consistent with that obtained from TEM image.

FT-IR spectroscopy was used to characterize the interaction among CS, MWCNT, CS-MWCNT, Fe_3O_4 NPs, and CS-MWCNT-Fe_3O_4 is shown in Fig. 1B. in the FT-IR spectrum of CS, the peaks at 3500–3300 cm^{-1} is attributing to —OH and —NH_2 group stretching vibration. The peaks at 1598 cm^{-1} and 1655 cm^{-1} are denoting to the $–NH_2$ and $–CONH_2$ group (types I and II) of the CS [22,29]. The peak at 1318 cm^{-1} and 1155 cm^{-1} are indicating to the stretching vibration of C–N (type amine I). In the FT–IR spectrum of the MWCNT, which does not appear in characterize peaks [38]. In the FT–IR spectrum of the MWCNT-CS, the new characterize peak is appeared corresponding to CS. This result suggested

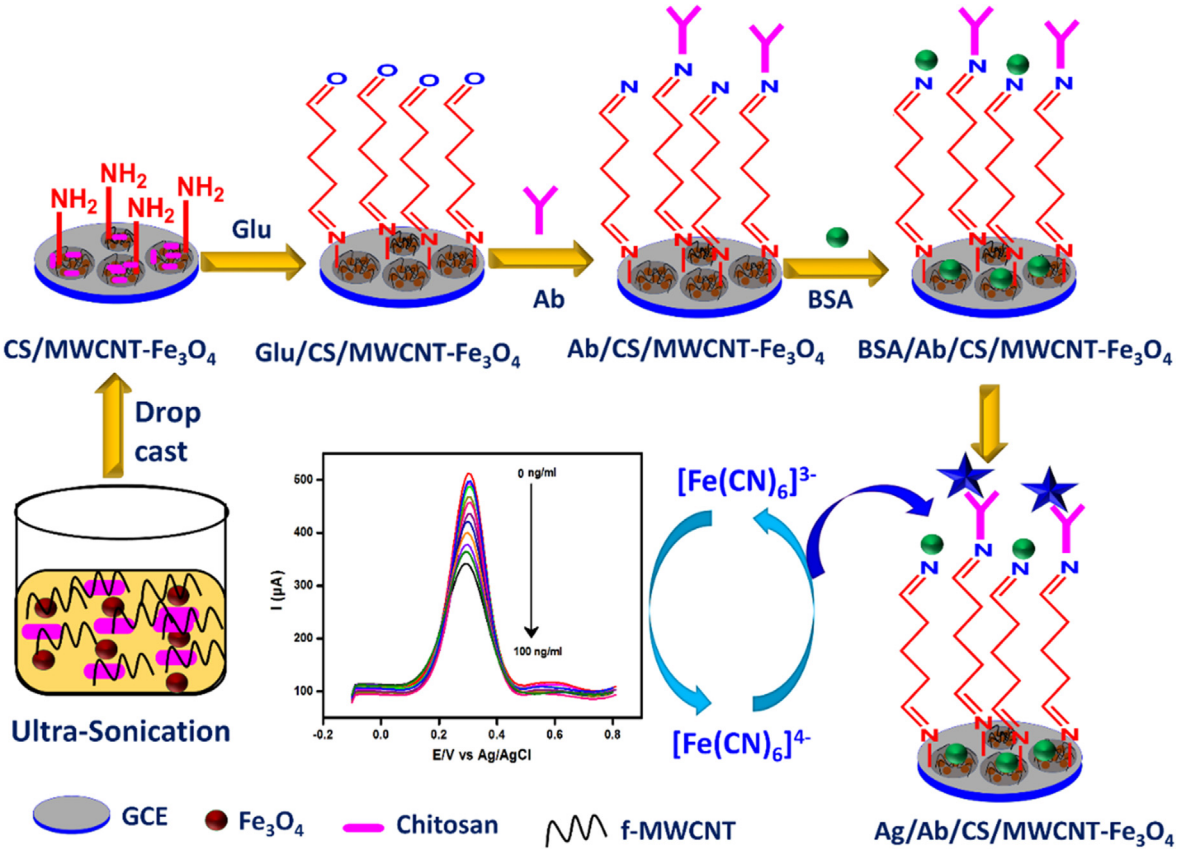

Scheme 1. Schematic illustration of step by step fabrication of CS-MWCNT-Fe_3O_4 immuno-electrode for electrochemical detection of CA19-9 antigen.

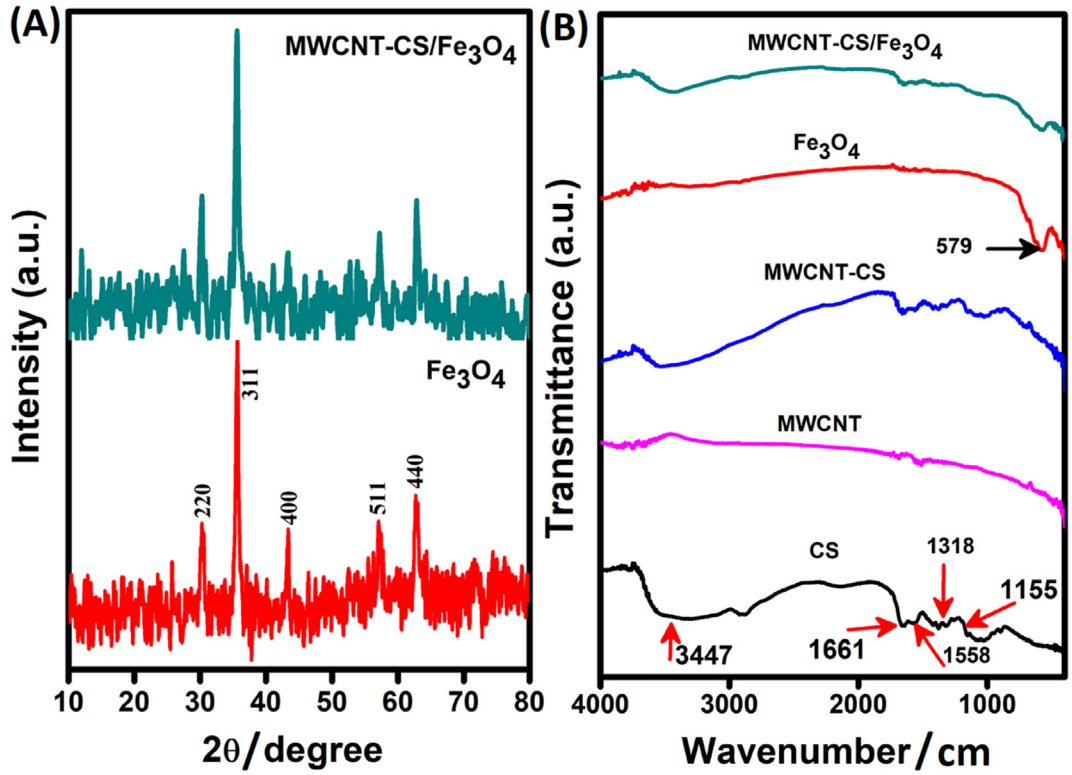

Fig. 1. (A) XRD spectrum of Fe_3O_4 and CS-MWCNT-Fe_3O_4 bio-nanocomposite, and (B) FT-IR spectrum of MWCNT, Fe_3O_4, MWCNT-CS, and CS-MWCNT-Fe_3O_4 bio-nanocomposites.

that CS is functionalized on the surface of MWCNT. In the FT-IR spectrum of the Fe_3O_4, the peak at 579 cm^{-1} attributed to Fe–O is stretching vibration [45]. The absorption peaks of CS-MWCNT-Fe_3O_4 composites are parallel to the CS – MWCNT and Fe_3O_4NPs.

Nitrogen (N_2) adsorption experiments were also used to studied the surface area of materials. Fig. S1 N_2 adsorption/desorption isotherms for MWCNT, Fe_3O_4, and CS-MWCNT-Fe_3O_4 displayed type II isotherms are shown in Fig. S1. As shown in Fig S1, the surface area of the MWCNT, Fe_3O_4, and CS-MWCNT-Fe_3O_4 was found to be 9.82, 10.29, and 8.79 m^2 g^{-1}, indicating after the chitosan modified composite was lower surface area. Chitosan was slightly blocked the pore size.

The morphology of composite was characterized by TEM techniques. As can be observed in Fig. 2A, the morphology of pristine MWCNT was an approximately uniform size distribution. As shown in Fig. 2B, the surface and size morphology of Fe_3O_4 NPs are porous structure and even spherical shape with a particle size of about 100 nm. As seen in Fig. 2C, the MWCNT is equally dispersed in the CS solution. Fig. 2D shows the CS-MWCNT-Fe_3O_4 bio-nanocomposites can be observed as spherical NPs where CS cross-linking between MWCNT and Fe_3O_4 NPs. On the other hand, as-formed CS was coated on the surface of Fe_3O_4 NPs and increasing the stability of composites.

3.2. Principle of electrochemical immunosensor

The principle of the developed electrochemical immunosensor is illustrated in Scheme 1. Nanocomposite films of CS-MWCNT/Fe_3O_4 was used to immobilize antibodies (anti-CA19-9) on electrode via glutaraldehyde and $[Fe(CN)_6]^{3-/4-}$ as redox probe., which increased the loading amount of antibody and facilitated the electron transfer. The interactions of antibody and antigen was recorded using square wave voltammetry (SWV) technique. The redox peak current was decreased when the antigen binds with antibody. Hence, the amount of CA 19–9 to react with the CA 19–9 antibody would decrease anodic peak currents of the $[Fe(CN)_6]^{3-/4-}$ because of an antigen blocked the electrode surface and, hindered the electron transfer. The SWV peak current displayed a good relationship with the amount of CA 19–9 antigen was captured by the electrode. By this label-free immunosensor principle, the calibration plot was constructed between CA 19–9 concentration and the anodic peak current of the SWV.

3.3. Electrochemical characterization of the immunosensor

The CV of fabricated immunosensor on GCE modified surface was determined by using 0.1 M KCl containing 0.01 M $[Fe(CN)_6]^{3-/4-}$ (0.05 M PBS, pH 7.4) (Fig. 3A). In Fig. 3A, observed CS-MWCNT-Fe_3O_4 modified electrode (curve b) current was increased compared with the bare GCE (curve a), demonstrating that composite can highly promote the electron transfer ability and enlarge the electrode surface area. After that CS-MWCNT-Fe_3O_4/GCE modified electrode was immersed in 2% of Glu solution, the peak was decreased (curve c), representing the successful attachment of Glu on the modified electrode surface. Then, the Anti-CA19-9 antibodies were immobilized on the Glu/CS-MWCNT-Fe_3O_4 modified

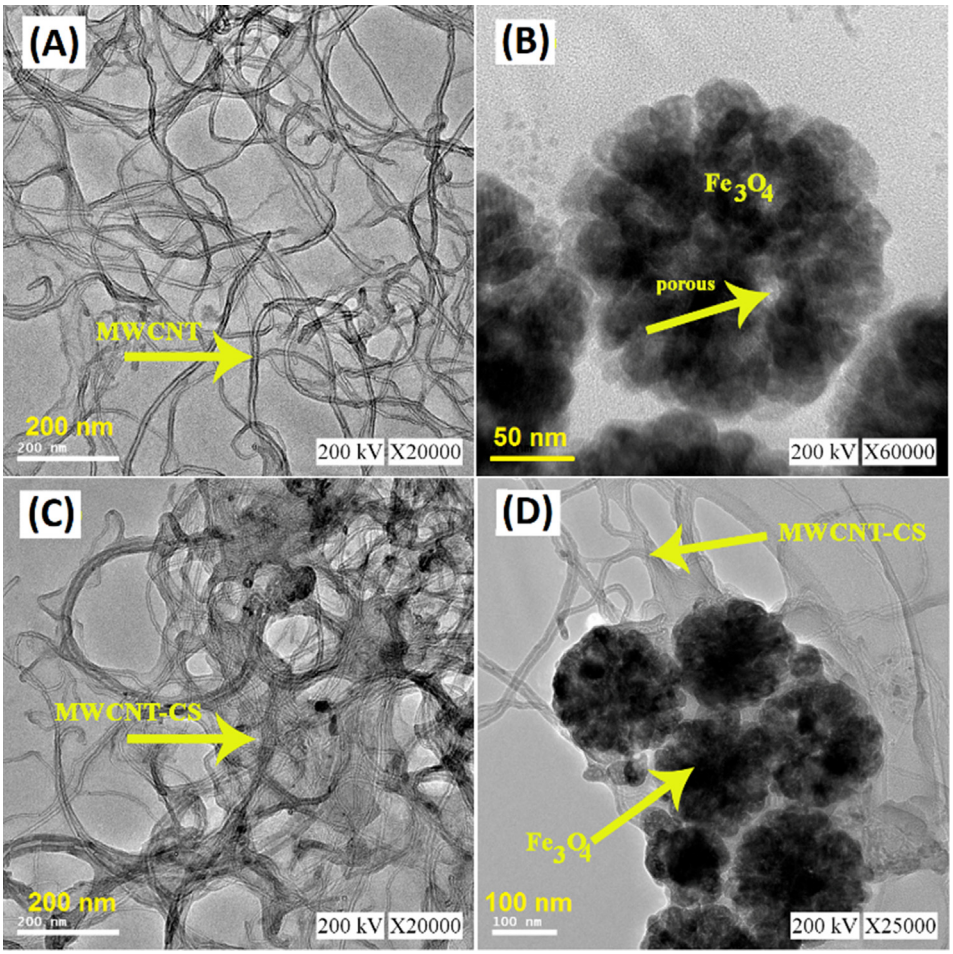

Fig. 2. TEM image of (A) MWCNT, (B) Fe_3O_4 NPs, (C) MWCNT-CS, and (D) CS-MWCNT-Fe_3O_4 bio-nanocomposites.

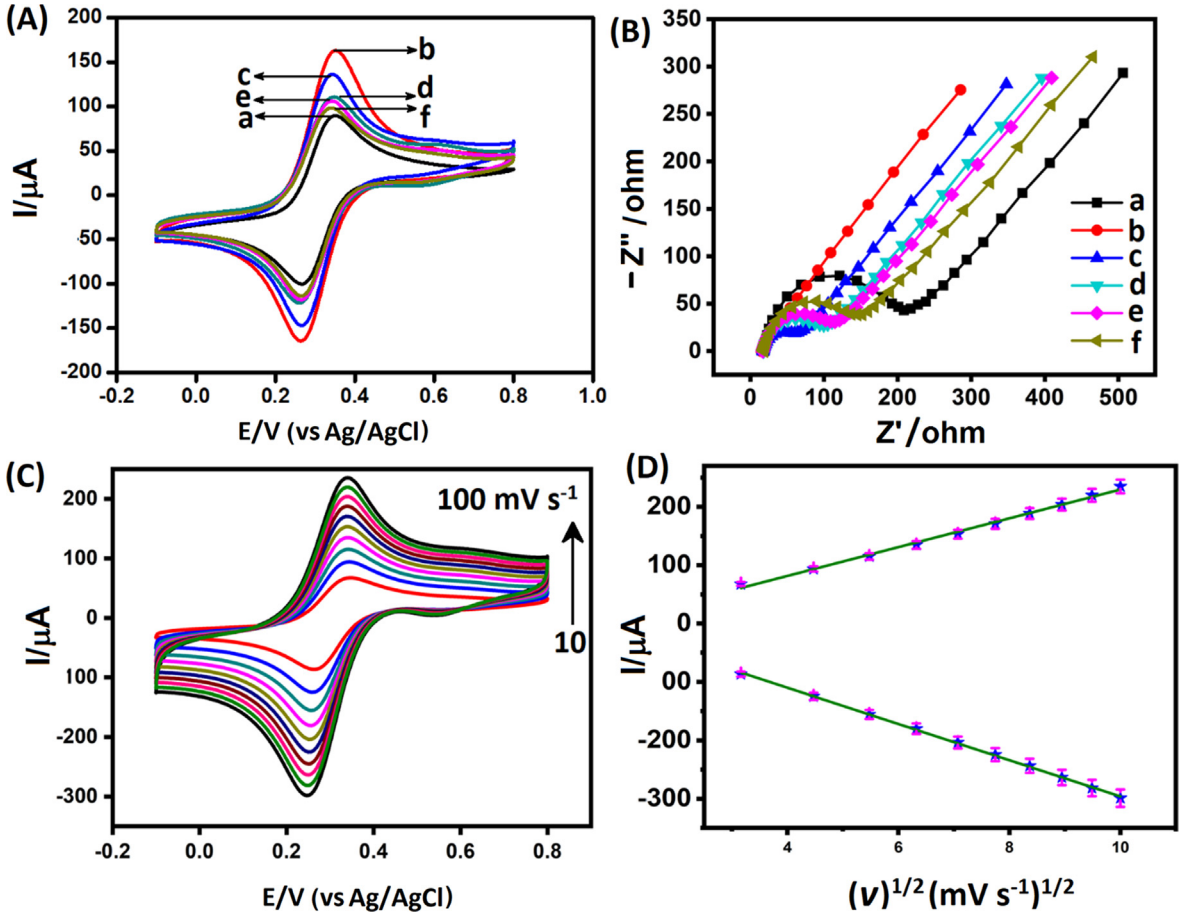

Fig. 3. (A) CVs profile, (B) EIS method (a) bare GCE, (b) CS-MWCNT-Fe_3O_4/GCE, (c) Glu/CS-MWCNT-Fe_3O_4/GCE, (d) Abs_{CA19-9}/CS-MWCNT-Fe_3O_4/GCE, (e) BSA/ Abs_{CA19-9}/CS-MWCNT-Fe_3O_4/GCE and (f) ag/BSA/ Abs_{CA19-9}/CS-MWCNT-Fe_3O_4/GCE, (C) CV performance of Ag/BSA/ AbsCA19-9/Glu/CS-MWCNT-Fe_3O_4/GCE in 0.05 M PBS containing 0.1 M $[Fe(CN)_6]^{3-/4-}$ and 0.1 M KCl at different scan rates (10–100 mV s^{-1}) and (D) Their corresponding correlation plot of cathodic and anodic peak current versus square root of scan rate over the modified electrodes: I_{pa} (μA) = 24.67X-17.03 (R^2 = 0.994), I_{pc} (μA) = -31.02X + 14.33 (R^2 = 0.998).

GCE, the redox peak current was decreased (curve d), which indicates the successful attachment of antibodies molecules on the Glu/CS-MWCNT-Fe_3O_4/GCE. After BSA was immobilized on the Abs_{CA19-9} modified electrode surface, peak current was decreased due to the blocking of remaining active sites against non-specific binding (curve e). Finally, the peak current decreased after CA 19–9 antigen was immobilized on the BSA/Abs_{CA19-9}/Glu/CS-MWCNT-Fe_3O_4/GCE electrode surface, because of CA 19–9 on the electrode hindered the electron transfer (curve f).

Additionally, electrochemical impedance spectroscopy (EIS) was also recorded at each step to examine the effect of interfacial state changes of the constructed immunosensor procedures (Fig. 3B). The semicircle portion reflects the electron-transfer resistance (R_{et}) of the $[Fe(CN)_6]^{3-/4-}$ (redox probe) at the electrode interfaces. As demonstrated the EIS of the bare GCE displayed a relatively larger semicircle (curve a) could be observed. After CS-MWCNT-Fe_3O_4 was drop cast on the GCE, the electron transfers resistance (R_{ct}) was decreased (curve b) compared with the bare GCE (curve a). This result proved that CS-MWCNT-Fe_3O_4 is an excellent electron transfer and the electric conductivity materials. Finally, stepwise immobilization of Glu, Abs_{CA19-9}, BSA, and Ag on the surface of a CS-MWCNT-Fe_3O_4/GCE, Ret value was increased (curves c, d, e, and f); the reason is that protein forms a non-conducting layer successfully binds on the CS-MWCNT-Fe_3O_4/GCE bio-nanocomposite surface.

Fig. 3C and Fig. S3A,C (supporting information) represents the CV results of studies conducted using immuno-electrode in $[Fe(CN)_6]^{3-/4-}$ (0.05 M PBS, pH 7.4) at different scan rates (0.01–0.1 V s^{-1}) were also studied with Ag/BSA/Abs_{CA19-9}/Glu/CS-MWCNT-Fe_3O_4/GCE, CS-MWCNT-Fe_3O_4/GCE and Abs_{CA19-9}/Glu/CS-MWCNT-Fe_3O_4/GCE. As a result, the cathodic and anodic peak current was gradually increased as a function of increasing scan rate (ν). Fig. 3D and S3B,D (supporting information) show the corresponding correlation plot of cathodic and anodic peak current vs square root of scan rate suggesting the modified electrode was diffusion-controlled redox process. The electroactive surface area of the modified electrodes can be calculated by using the following equation [46].

$$I_p = 2.69 \times 10^5 A \times D^{1/2} n^{3/2} C \nu^{1/2} \quad (2)$$

where I_p, A, and D represents the maximum current (A), electrode surface area (cm^2), and diffusion coefficient, respectively n is the number of electrons transferred in redox event, C is the concentration of redox material, and v is the scan rate (V/s). The average surface electroactive area of bare GCE, Fe_3O_4, MWCNT-CS, CS-MWCNT-Fe_3O_4 and Ag/BSA/Abs_{CA19-9}/Glu/CS-MWCNT-Fe_3O_4 modified GCE were calculated as 0.072 cm^2, 0.095 cm^2, 0.53 cm^2, 1.14 cm^2, and 0.75 cm^2, respectively. The result suggests that CS-MWCNT-Fe_3O_4 modified electrode has a high electroactive surface area, which is also used by the analytical sensing platform. Then, the Ag modified electrode was decreased the active surface area due to the non-conducting antigen (Ag) was blocking the active area, which is confirmed Ag was immobilized on the final modification electrode surface.

3.4. Optimization of operational parameter for CA19-9 immune-sensing CA 19–9 antigen

The proposed immunosensor was optimized by different parameters such as pH, the incubation time of antibody, concentration of antibody, incubation temperature, and Ag-Ab incubation time of the BSA/Abs_{CA19-9}/Glu/CS-MWCNT-Fe_3O_4/GCE electrode for better performance. The pH was a major impact on the biosensor because it can influence the electrochemical behavior of film and stability of immobilized antibodies [47]. The immunosensor was responded at 10 μg mL^{-1} of CA 19–9 in different pH (6.1, 6.5, 7.0, 7.4, 7.6, and 8.0) containing 0.01 M $[Fe(CN)_6]^{3-/4-}$/0.1 M KCl solution as shown in Fig. 4A. The pH increases from 6.0 to 7.4 with a slow decrease in the peak current. The peak current was slightly increased with an increase in pH range from 7.4 to 8.0. These results are demonstrating that the anti-CA19-9 antibody was denatured in a strongly acidic or alkaline solution Thus pH = 7.4 was suitable for CA 19–9 immunosensor.

The effect of temperature on the immunosensor performance was examined at the incubation temperature range from 5 to 40 °C. The result displayed that the suitable temperature for the Ab-Ag interaction would be 35 °C (Fig. 4E). In high incubation temperature, peak current increased. This result suggests that it may be due to the denaturation of protein.

Optimization of antibody incubation time and concentration of antibody immobilized on the Glu/CS-MWCNT-Fe_3O_4 electrode surface was recorded by SWV. The Glu/CS-MWCNT-Fe_3O_4 /GCE electrode was incubated at 2 μg mL^{-1} at different times. The peak current was decreased when the incubation time was increased from 5 to 40 min and then remained unchanged at longer incubation times (Fig. 4B). The result indicating that the immobilization of antibody on the electrode surface has reached the saturation level in 40 min. So, 40 min of optimal incubation time was selected. Related to the immobilization of the capture anti-CA19-9 on the electrode surface, different concentrations of antibody solution were tested in Fig. 4C. The peak current was decreased with the increasing antibody concentration from 2 to 16 μg mL^{-1}. This is due to the successful attachment of anti-CA19-9 antibody that reduces the electron transfer from the redox solution to the electrode surface. The current was constant with the further increasing concentration of antibody (Fig. 4D). So, 16 μg mL^{-1} was used as an optimum concentration of antibody for CA 19–9 immunosensor. To investigate the optimized incubation time for the formation of antigen and antibody immuno-complex, the fabricated immunosensor was incubated for various times in the presence of 10 ng mL^{-1} CA 19–9 (Fig. 4F). The higher response current was observed in 30 min, after which the incubation time continued to increase, the current response approximately constant. This result indicates that 30 min was optimum incubation time for antigen and antibody.

3.5. Electrochemical immune-sensing of the CA19-9 antigen

The analytical performance of CA19-9 immunosensor was examined under the optimum condition (pH: 7.4, antibody incubation

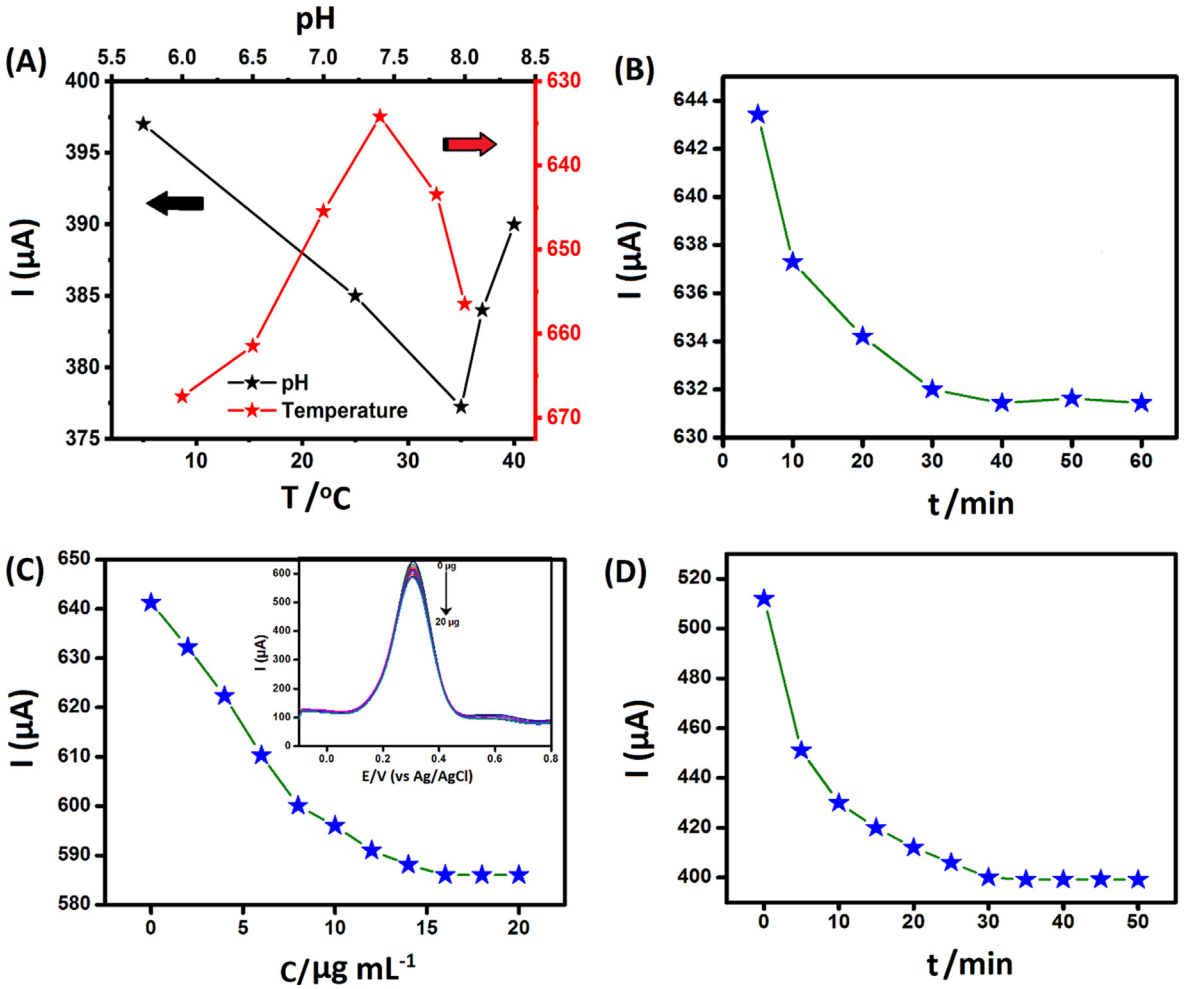

Fig. 4. The effect of a key factor on the CA 19–9 currents of the immunosensor in 0.05 M PBS containing 0.01 M $[Fe(CN)_6]^{3-/4-}$/0.1 M KCl: (A) Influence of pH (0.05 M PBS) and the temperature effect, (B) Ab incubation time, (C) Ab concentrations (0–20 μg), and (E) Ag incubation time. All measurements were repeated three times (n = 3).

time: 40 min, antibody concentration: 16 μg mL^{-1}, incubation temperature: 35 °C, and antigen and antibody binding time: 30). Fig. 5A displays the SWV curves, the peak current response of the proposed immunosensor after the Ag–Ab immuno-reaction. It shows the concentration range from 0.001 to100 ng mL^{-1}, the peak current decreased with the increasing concentration of CA 19–9 antigen, which clearly shows a "signal off" trend, and this result proofing that CA 19–9 antigen successfully binds with the CA 19–9 antibody on the surface of the electrode (Fig. 5A). In Fig. 5B, the linear regression equation was $(I_{p0}–I_p)/I_{p0}$ = 0.1839 [$\log_{CA19-9}$] + 0.7822, and coefficient R^2 = 0.994. The fabricated immunosensor shows a good linear range from 0.001 to 100 ng mL^{-1} (Fig. 5B) with a LOD was 0.163 pg mL^{-1}(S/N = 3) and the threshold value of less than 3 ng mL^{-1} for clinical diagnosis. The analytical parameter of the fabricated immunosensor has been compared with the recently reported CA 19–9 detection studies as shown in Table 1 [48–56].

3.6. Selectivity, reproducibility and stability of the immuno-sensor

The interference study was evaluated by incubation of different proteins upon the proposed immunosensor. CA 125, AFP, and CEA are the main interfering proteins for proposed immunosensor. We conducted the immunosensor experiment as interfering proteins (100 ng mL^{-1}) mixed with pure CA 19–9 (10 ng mL^{-1}) solution. Fig. 6A shows that a clearly higher signal change can be found for the CA 19–9 than the interfering proteins. Those current changes were less than 5% without interference proteins suggesting a good selectivity of the immunosensor for CA 19–9. To evaluate the reproducibility of the immunosensor, four electrodes were constructed for the detection of CA 19–9 (10 ng mL^{-1}) under the optimum conditions (Fig. 6B). The relative standard deviation (RSD) of the response current signal for immunosensor was around 3.4% revealing good accuracy and reproducibility of the immunosensor. Furthermore, we obtained that the immunosensor retained 99% of the original peak current after storage in pH 7.4 PBS at 4 °C for 15 days, this result demonstrating the good self-storage stability of the proposed immunosensor in Fig. 6C.

3.7. Sensing performance evaluation using real serum samples

The proposed immunosensor was challenged by detecting serum samples from endometriosis patients. Thus, 5, 10, 15 and 20 ng of recombinant CA19-9 antigen was added into serum blood, which was measured by SWV (Table 2). After BSA/Abs_{CA19-9}/Glu/CS-MWCNT-Fe_3O_4/GCE electrode directly used for the detection of CA 19–9 antigen from control and endometriosis serum.

The serum samples were diluted by 100-times of PBS (pH 7.4). The CA19-9 concentration was measured by the proposed method and compared with ELISA (Fig. 5). As shown in Tables 2 and Table 3, our proposed immunoassay results displayed parallel with ELISA. The developed immunosensor showed RSD value of 6.6% and ELISA method as RSD value of 7.3%. According to these results, the proposed immuno-assay has potential applications for diagnosis of endometriosis.

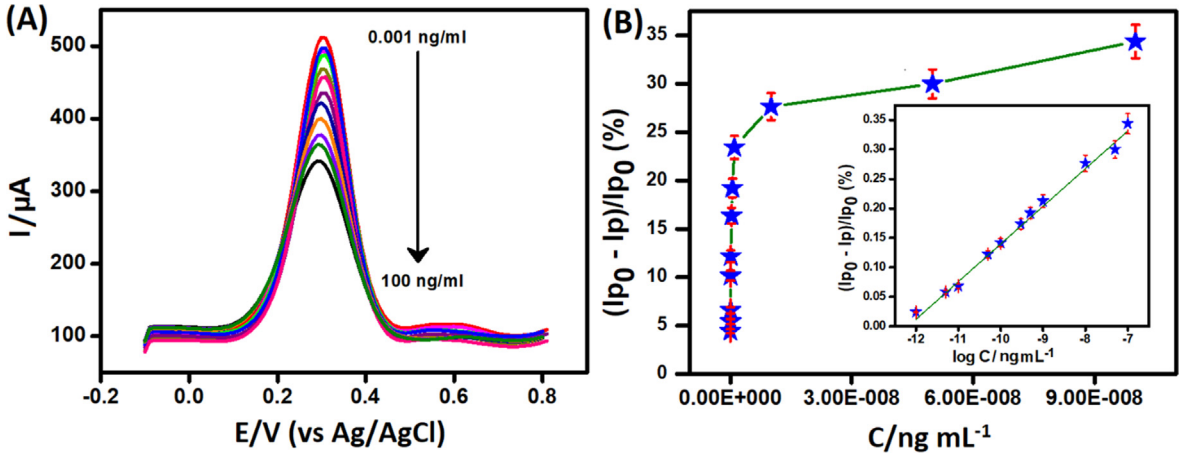

Fig. 5. (A) The SWV response of the immunosensor after incubating with different concentrations of CA 19–9 (0 ng mL^{-1} to 100 ng mL^{-1}), and (B) Calibration curve of the CA 19–9 representing the oxidation peak current of $[Fe(CN)_6]^{3-/4-}$ as a function of CA 19–9 concentration, the peak currents versus the logarithms of CA 19–9 concentrations were linearly correlated; $(I_{p0}–I_p)/I_{p0}$ = 0.1839 [$\log_{CA19-9}$] + 0.7822, and coefficient R^2 = 0.994 (Inset). All measurements were repeated three times (n = 3).

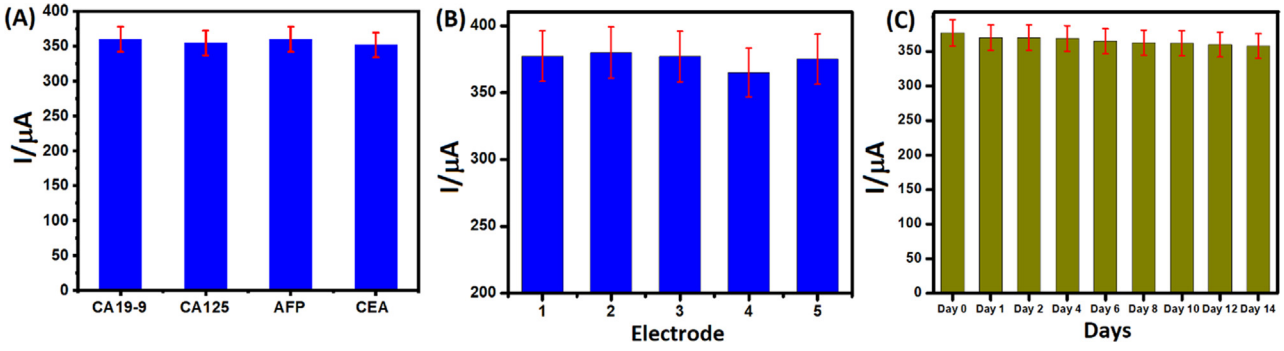

Fig. 6. (A) The current response of fabricated immunosensor in the presence of the 10 ng mL^{-1} CA 19–9, 10 ng mL^{-1} CA 19–9 + 100 ng mL^{-1} CA 125, 10 ng mL^{-1}CA 19–9 + 100 ng mL^{-1}AFP, 10 ng mL^{-1} CA 19–9 + 100 ng mL^{-1}CEA, (B) SWV response of corresponding reproducibility of different electrode, and (C) storage stability (error bar, RSD (n = 3)).

Table 2
Electrochemical detection of CA19-9 in human blood samples.

Source	Proposed sensor			Reference method ELISA	
	Added (pg mL^{-1})	Found (pg mL^{-1})	Std. dev. (n = 3)	Found (pg mL^{-1})	Std. dev. (n = 3)
Human serum samples	5	4.8	0.270	4.7	0.421
	10	9.5	0.141	9.3	0.083
	15	14.1	0.158	14.5	0.758
	20	19.1	0.258	19.5	0.480

Table 3
Electrochemical detection of CA19-9 in endometriosis serum samples (clinical blood).

Source	Proposed sensor		Reference method ELISA	
	Found (ng mL^{-1})	Std. dev. (n = 3)	Found (ng mL^{-1})	Std. dev. (n = 3)
Healthy patient	3.5	0.234	3	0.685
Endometriosis patient (Stage-I)	12	0.990	11	1.717
Endometriosis patient (Stage-II)	25	1.324	24.5	1.414
Endometriosis patient (Stage-III)	38	1.167	37	1.740
Endometriosis patient (Stage-IV)	55	2.112	58	2.178

4. Conclusion

In summary, this research for the first time reported the fabrication of CS-MWCNT-Fe_3O_4 bio-nanocomposite based electrochemical immunosensor for label-free, selective and sensitive detection of CA19-9 analyte, a potential biomarker for endometriosis diagnostics application. This novel and efficient CA19-9 immunosensor exhibited a LOD of 0.163 pg mL^{-1} and a wide detection range varies from 0.001 to 100 ng mL^{-1} of CA19-9 concentration. The observed enhanced and desired sensing performance is due to the synergism effect of high catalytic activity of Fe_3O_4 and the high conductivity of MWCNT with good bio-adsorption of chitosan. This method shows high sensitivity and quick detection of CA19-9 biomarker. Our developed method for electrochemical immuno-sensing of CA19-9 is affordable and scalable to the clinical application if compared with ELISA. To claim the clinical utilization of this smart sensor, we tested out sensors using real samples, and outcomes were validated using ELISA. This project bio-nanocomposites based electrochemical CA19-9 immuno-sensor for endometriosis diagnostics application, even at point-of-care application. As salient features, such CA19-9 sensing system is selective, accurate with precision, display results rapidly, affordable, and very importantly easy to fabricate. Towards translational aspects, we are optimizing possibilities to connect this smart sensor with micro-electronics to developing a portable CA19-9 immuno-sensing system needed for on-site diagnostics application.

Declaration of Competing Interest

The authors declare that they have no known competing financial interests or personal relationships that could have appeared to influence the work reported in this paper.

Acknowledgments

The study was financially supported by the Department of Science and Technology (DST-SERB), New Delhi, India. File no: ECR/2016/001664/LS (Date: 29-Mar-2017).

Appendix A. Supplementary material

Supplementary data to this article can be found online at https://doi.org/10.1016/j.bioelechem.2021.107740.

References

[1] G. Bin Yang, Clinical value of serum cancer antigen 19–9 as a tumor screening marker among healthy individuals, J. B.U.ON. 20 (2015) 1612–1616.
[2] Z. Kurdoglu, R. Gursoy, M. Kurdoglu, M. Erdem, O. Erdem, A. Erdem, Comparison of the clinical value of CA 19–9 versus CA 125 for the diagnosis of endometriosis, Fertil. Steril. 92 (2009) 1761–1763.
[3] A. Manousopoulou, M. Hamdan, M. Fotopoulos, D.J. Garay-Baquero, J. Teng, S.D. Garbis, Y. Cheong, Integrated Eutopic Endometrium and Non-Depleted Serum Quantitative Proteomic Analysis Identifies Candidate Serological Markers of Endometriosis, Proteomics - Clin. Appl. 13 (2019) 1–8.
[4] D. Pandey, P. Wasinghon, K.G. Huang, Laparoscopic Management of Peritonitis Due to a Ruptured Ovarian Endometrioma with Extremely High Levels of Cancer Antigen-125 and Cancer Antigen-19-9, J. Gynecol. Surg. 35 (2019) 198–200.
[5] S. Pils, C. Paternostro, M.E. Mayerhoefer, A. Reinthaller, M. Feichtinger, Heavy black tea consumption and elevated CA 19–9 and CA 125 levels. A case report on a patient with ovarian endometriotic cysts, Gynecol. Endocrinol. 35 (2019) 478–480.
[6] J.C. Soares, L.E.O. Iwaki, A.C. Soares, V.C. Rodrigues, M.E. Melendez, J.H.T.G. Fregnani, R.M. Reis, A.L. Carvalho, D.S. Correa, O.N. Oliveira, Immunosensor for pancreatic cancer based on electrospun nanofibers coated with carbon nanotubes or gold nanoparticles, ACS Omega. 2 (2017) 6975–6983.
[7] N. Kaewwonglom, M. Oliver, D.J. Cocovi-Solberg, K. Zirngibl, D. Knopp, J. Jakmunee, M. Miró, Reliable Sensing Platform for Plasmonic Enzyme-Linked Immunosorbent Assays Based on Automatic Flow-Based Methodology, Anal. Chem. 13260–13267 (2019).
[8] L. Jiao, L. Zhang, W. Du, H. Li, D. Yang, C. Zhu, Au@Pt nanodendrites enhanced multimodal enzyme-linked immunosorbent assay, Nanoscale 11 (2019) 8798–8802.
[9] Y. Zhao, W. Gao, X. Ge, S. Li, D. Du, H. Yang, Analytica Chimica Acta CdTe@SiO_2 signal reporters-based fluorescent immunosensor for quantitative detection of prostate specific antigen, Anal. Chim. Acta 1057 (2019) 44–50.
[10] X. Zhang, S. Liu, J. Pan, H. Jia, Z. Chen, T. Guo, Multifunctional oligomer immobilized on quartz crystal microbalance: a facile and stabilized molecular imprinting strategy for glycoprotein detection, Anal. Bioanal. Chem. 411 (2019) 3941–3949.
[11] B. Zhou, Y. Hao, S. Chen, P. Yang, A quartz crystal microbalance modified with antibody-coated silver nanoparticles acting as mass signal amplifiers for real-time monitoring of three latent tuberculosis infection biomarkers, Microchim. Acta. 186 (2019) 212.
[12] J. Zhou, N. Gan, T. Li, H. Zhou, X. Li, Y. Cao, L. Wang, Chemical Ultratrace detection of C-reactive protein by a piezoelectric immunosensor based on Fe_3O_4@SiO_2 magnetic capture nanoprobes and HRP-antibody co-immobilized nano gold as signal tags, Sens. Actuat. B Chem. 178 (2013) 494–500.

[13] E. Makhneva, Z. Farka, M. Pastucha, A. Obrusník, V. Horáčková, P. Skládal, L. Zajíčková, Maleic anhydride and acetylene plasma copolymer surfaces for SPR immunosensing, Anal. Bioanal. Chem. 411 (2019) 7689–7697.
[14] S. Nootchanat, W. Jaikeandee, P. Yaiwong, C. Lertvachirapaiboon, K. Shinbo, K. Kato, S. Ekgasit, A. Baba, Fabrication of miniature surface plasmon resonance sensor chips by using confined sessile drop technique, ACS Appl. Mater. Interfaces. 11 (2019) 11954–11960.
[15] N. Ma, T. Zhang, T. Yan, X. Kuang, H. Wang, D. Wu, Q. Wei, Novel electrochemical immunosensor for sensitive monitoring of cardiac troponin I using antigen–response cargo released from mesoporous Fe_3O_4, Biosens. Bioelectron. 143 (2019) 111608.
[16] Y.K. Goud, S.V. Kumar, A. Hayat, V.K. Gobi, H. Song, K.H. Kim, J.L. Marty, A highly sensitive electrochemical immunosensor for zearalenone using screen-printed disposable electrodes, J. Electroanal. Chem. 832 (2019) 336–342.
[17] J. Zhang, R. Jin, D. Jiang, H.-Y. Chen, Electrochemiluminescence-based capacitance microscopy for label-Free Imaging of antigens on the cellular plasma membrane, J. Am. Chem. Soc. 141 (2019) 10294–10299.
[18] E.K.G. Trindade, B.V.M. Silva, R.F. Dutra, A probeless and label-free electrochemical immunosensor for cystatin C detection based on ferrocene functionalized-graphene platform, Biosens. Bioelectron. 138 (2019) 111311.
[19] B. Jeong, R. Akter, O.H. Han, C.K. Rhee, M.A. Rahman, Increased electrocatalyzed performance through dendrimer-encapsulated gold nanoparticles and carbon nanotube-assisted multiple bienzymatic labels: Highly sensitive electrochemical immunosensor for protein detection, Anal. Chem. 85 (2013) 1784–1791.
[20] M. Zhang, W. Gorski, Electrochemical sensing platform based on the carbon nanotubes/redox mediators-biopolymer system, J. Am. Chem. Soc. 127 (2005) 2058–2059.
[21] A. Tabasi, A. Noorbakhsh, E. Sharifi, Reduced graphene oxide-chitosan-aptamer interface as new platform for ultrasensitive detection of human epidermal growth factor receptor 2, Biosens. Bioelectron. 95 (2017) 117–123.
[22] S. Prakash, T. Chakrabarty, A.K. Singh, V.K. Shahi, Silver nanoparticles built-in chitosan modified glassy carbon electrode for anodic stripping analysis of As (III) and its removal from water, Electrochim. Acta. 72 (2012) 157–164, https://doi.org/10.1016/j.electacta.2012.04.025.
[23] M.F. Wu, Y. Wang, S. Li, X.X. Dong, J.Y. Yang, Y.D. Shen, H. Wang, Y.M. Sun, H.T. Lei, Z.L. Xu, Ultrasensitive immunosensor for acrylamide based on chitosan/SnO_2-SiC hollow sphere nanochains/gold nanomaterial as signal amplification, Anal. Chim. Acta. 1049 (2019) 188–195.
[24] R. Devi, S. Gogoi, S. Barua, H. Sankar Dutta, M. Bordoloi, R. Khan, Electrochemical detection of monosodium glutamate in foodstuffs based on Au@MoS_2/chitosan modified glassy carbon electrode, Food Chem. 276 (2019) 350–357.
[25] P. Samadi Pakchin, H. Ghanbari, R. Saber, Y. Omidi, Electrochemical immunosensor based on chitosan-gold nanoparticle/carbon nanotube as a platform and lactate oxidase as a label for detection of CA125 oncomarker, Biosens. Bioelectron. 122 (2018) 68–74.
[26] L. Tian, J. Qi, K. Qian, O. Oderinde, Y. Cai, C. Yao, W. Song, Y. Wang, An ultrasensitive electrochemical cytosensor based on the magnetic field assisted binanozymes synergistic catalysis of Fe_3O_4 nanozyme and reduced graphene oxide/molybdenum disulfide nanozyme, Sensors Actuat. B Chem. 260 (2018) 676–684.
[27] W. Zhu, M. Saddam Khan, W. Cao, X. Sun, H. Ma, Y. Zhang, Q. Wei, Ni$(OH)_2$/NGQDs-based electrochemiluminescence immunosensor for prostate specific antigen detection by coupling resonance energy transfer with Fe_3O_4@MnO_2 composites, Biosens. Bioelectron. 99 (2018) 346–352, https://doi.org/10.1016/j.bios.2017.08.005.
[28] Y. Wang, G. Zhao, Y. Zhang, X. Pang, W. Cao, B. Du, Q. Wei, Sandwich-type electrochemical immunosensor for CEA detection based on Ag/MoS_2@Fe_3O_4 and an analogous ELISA method with total internal reflection microscopy, Sens. Actuators B Chem. 266 (2018) 561–569.
[29] S. Lv, J. Sheng, S. Zhao, M. Liu, L. Chen, The detection of brucellosis antibody in whole serum based on the low-fouling electrochemical immunosensor fabricated with magnetic Fe_3O_4@Au@PEG@HA nanoparticles, Biosens. Bioelectron. 117 (2018) 138–144.
[30] L.T. Tufa, S. Oh, V.T. Tran, J. Kim, K.J. Jeong, T.J. Park, H.J. Kim, J. Lee, Electrochemical immunosensor using nanotriplex of graphene quantum dots, Fe_3O_4 and Ag nanoparticles for tuberculosis, Electrochim. Acta. 290 (2018) 369–377.
[31] M. Zhang, A. Smith, W. Gorski, Carbon nanotube– chitosan system for electrochemical sensing based on dehydrogenase enzymes, Anal. Chem. 76 (2004) 5045–5050.
[32] H. Beheshti, M. Irani, L. Hosseini, A. Rahimi, M. Aliabadi, Removal of Cr (VI) from aqueous solutions using chitosan/MWCNT/Fe_3O_4 composite nanofibers-batch and column studies, Chem. Eng. J. 284 (2016) 557–564.
[33] H. Wei, E. Wang, Fe_3O_4 magnetic nanoparticles as peroxidase mimetics and their applications in H_2O_2 and glucose detection, Anal. Chem. 80 (2008) 2250–2254.
[34] L. Yang, X. Ren, F. Tang, L. Zhang, A practical glucose biosensor based on Fe_3O_4 nanoparticles and chitosan/nafion composite film, Biosens. Bioelectron. 25 (2009) 889–895.
[35] N. Prabhakar, H. Thakur, A. Bharti, N. Kaur, Chitosan-iron oxide nanocomposite based electrochemical aptasensor for determination of malathion, Anal. Chim. Acta. 939 (2016) 108–116.
[36] G. Zhao, Q. Xu, Q. Zhang, Y. Guo, X. Sun, X.Y. Wang, Study on aptasensors modified by ionic liquid-Fe_3O_4 based on microarray electrodes for tetracycline detection, Int. J. Electrochem. Sci. 11 (2016) 1699–1706.
[37] S. Xu, S. Jiang, T. Wang, S. Guo, Effect of Fe_3O_4 on properties of carbon molecular sieves, J. Fuel Chem. Technol. 26 (1998) 375–376.
[38] J. de O. Marques Neto, C.R. Bellato, D. de C. Silva, Iron oxide/carbon nanotubes/chitosan magnetic composite film for chromium species removal, Chemosphere. 218 (2019) 391–401.
[39] Z. Xu, X. Fan, Q. Ma, B. Tang, Z. Lu, J. Zhang, G. Mo, J. Ye, J. Ye, A sensitive electrochemical sensor for simultaneous voltammetric sensing of cadmium and lead based on Fe_3O_4/multiwalled carbon nanotube/laser scribed graphene composites functionalized with chitosan modified electrode, Mater. Chem. Phys. 238 (2019) 121877.
[40] A. Sangili, M. Annalakshmi, S.M. Chen, P. Balasubramanian, M. Sundrarajan, Synthesis of silver nanoparticles decorated on core-shell structured tannic acid-coated iron oxide nanospheres for excellent electrochemical detection and efficient catalytic reduction of hazardous 4-nitrophenol, Compos. Part B Eng. 162 (2019) 33–42.
[41] R. Podgornik, M. Ličer, Polyelectrolyte bridging interactions between charged macromolecules, Curr. Opin. Colloid Interface Sci. 11 (2006) 273–279.
[42] S. Prakash, T. Chakrabarty, A.M. Rajesh, V.K. Shahi, Investigation of polyelectrolyte for electrochemical detection of uric acid in presence of ascorbic acid, Measurement 45 (2012) 500–506.
[43] C.R. Raj, K. Tokuda, T. Ohsaka, Electroanalytical applications of cationic self-assembled monolayers: square-wave voltammetric determination of dopamine and ascorbate, Bioelectrochemistry 53 (2001) 183–191.
[44] M. Dutta, B. Singh, M. Joshi, D. Das, E. Subramani, M. Maan, S.K. Jana, U. Sharma, S. Das, S. Dasgupta, C.D. Ray, B. Chakravarty, K. Chaudhury, Metabolomics reveals perturbations in endometrium and serum of minimal and mild endometriosis, Sci. Rep. 8 (2018) 1–9.
[45] A. Sangili, T. Kalyani, S.M. Chen, A. Nanda, S.K. Jana, Label-free electrochemical Immunosensor Based on One-Step Electrochemical Deposition of AuNPs-RGO nanocomposites for Detection of Endometriosis marker CA 125, ACS Appl. Bio Mater. 3 (2020) 7620–7630.
[46] A. Sangili, P. Veerakumar, S.M. Chen, C. Rajkumar, K.C. Lin, Voltammetric determination of vitamin B2 by using a highly porous carbon electrode modified with palladium-copper nanoparticles, Microchim. Acta 186 (2019) 299.
[47] Z. Dai, F. Yan, J. Chen, H. Ju, Reagentless amperometric immunosensors based on direct electrochemistry of horseradish peroxidase for determination of carcinoma antigen-125, Anal. Chem. 75 (2003) 5429–5434.
[48] X. Weng, Y. Liu, Y. Xue, A.J. Wang, L. Wu, J.J. Feng, L-Proline bio-inspired synthesis of AuPt nanocalliandras as sensing platform for label-free electrochemical immunoassay of carbohydrate antigen 19–9, Sens. Actuat. B Chem. 250 (2017) 61–68.
[49] M. Shi, S. Zhao, Y. Huang, L. Zhao, Y.M. Liu, Signal amplification in capillary electrophoresis based chemiluminescent immunoassays by using an antibody-gold nanoparticle-DNAzyme assembly, Talanta 124 (2014) 14–20.
[50] F. Yang, Z. Yang, Y. Zhuo, Y. Chai, R. Yuan, Ultrasensitive electrochemical immunosensor for carbohydrate antigen 19–9 using Au/porous graphene nanocomposites as platform and Au@Pd core/shell bimetallic functionalized graphene nanocomposites as signal enhancers, Biosens. Bioelectron. 66 (2015) 356–362.
[51] Y. Sha, Z. Guo, B. Chen, S. Wang, G. Ge, B. Qiu, X. Jiang, A one-step electrochemiluminescence immunosensor preparation for ultrasensitive detection of carbohydrate antigen 19–9 based on multi-functionalized graphene oxide, Biosens. Bioelectron. 66 (2015) 468–473.
[52] H. Zhu, G.C. Fan, E.S. Abdel-Halim, J.R. Zhang, J.J. Zhu, Ultrasensitive photoelectrochemical immunoassay for CA19-9 detection based on CdSe@ZnS quantum dots sensitized TiO_2NWs/Au hybrid structure amplified by quenching effect of Ab^2@V^{2+} conjugates, Biosens. Bioelectron. 77 (2016) 339–346.
[53] A. Zhang, H. Xiang, X. Zhang, W. Guo, E. Yuan, C. Huang, N. Jia, A novel sandwich electrochemiluminescence immunosensor for ultrasensitive detection of carbohydrate antigen 19–9 based on immobilizing luminol on Ag at BSA core/shell microspheres, Biosens. Bioelectron. 75 (2016) 206–212.
[54] M. Wang, M. Hu, B. Hu, C. Guo, Y. Song, Q. Jia, L. He, Z. Zhang, S. Fang, Bimetallic cerium and ferric oxides nanoparticles embedded within mesoporous carbon matrix: Electrochemical immunosensor for sensitive detection of carbohydrate antigen 19–9, Biosens. Bioelectron. 135 (2019) 22–29.
[55] X. Zhang, H. Ke, Z. Wang, W. Guo, A. Zhang, C. Huang, N. Jia, An ultrasensitive multi-walled carbon nanotube-platinum-luminol nanocomposite-based electro chemiluminescence immunosensor, Analyst. 142 (2017) 2253–2260.
[56] D. Wang, N. Gan, J. Zhou, P. Xiong, Y. Cao, T. Li, D. Pan, S. Jiang, Signal amplification for multianalyte electrochemical immunoassay with bidirectional stripping voltammetry using metal-enriched polymer nanolabels, Sens. Actuat. B Chem. 197 (2014) 244–253.